Fig 1A

$$\vec{F}_{rad} = 0$$
$$T = 2 \cdot |\vec{F}| \cdot r$$

Fig 1B
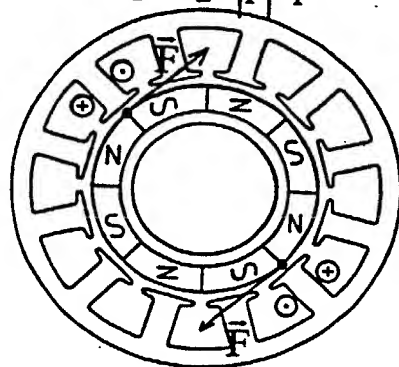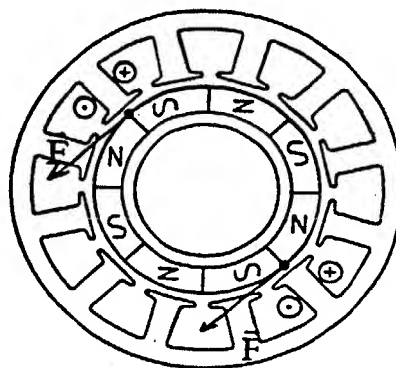
$$\vec{F}_{rad} = 2 \cdot \vec{F}$$
$$T = 0$$

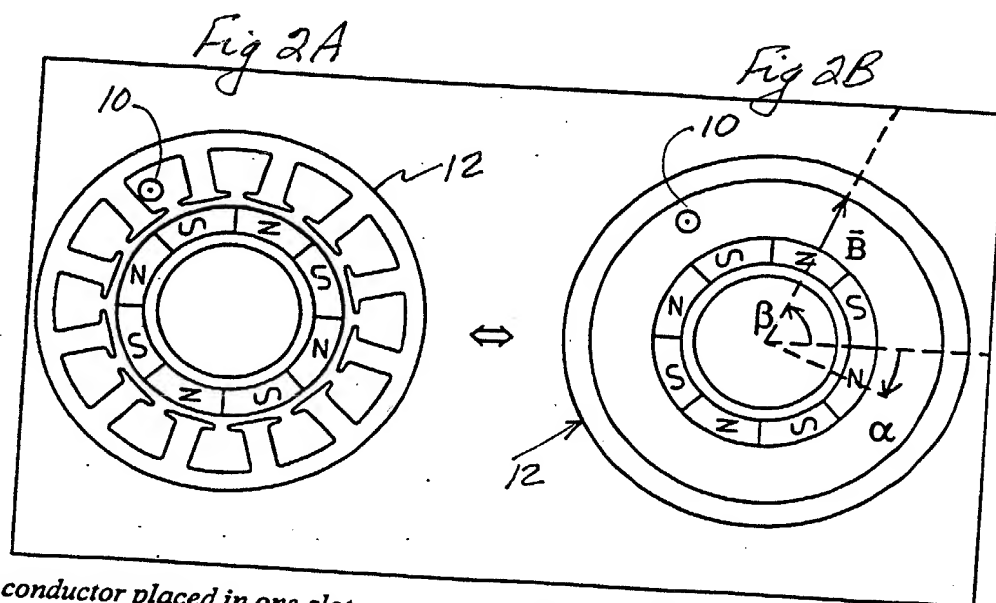a: 2 coils generating torque

b: 2 coils generating radial force

Fig. A.1

Fig 2A

Fig 2B

10

12

10

$\bar{B}$

β

α

12

a: conductor placed in one slot

b: assumption that conductor is placed in the airgap

Fig. A.3

Fig. 3A

$$|\vec{F}| = |\vec{B}| \cdot I \cdot l_{act}$$
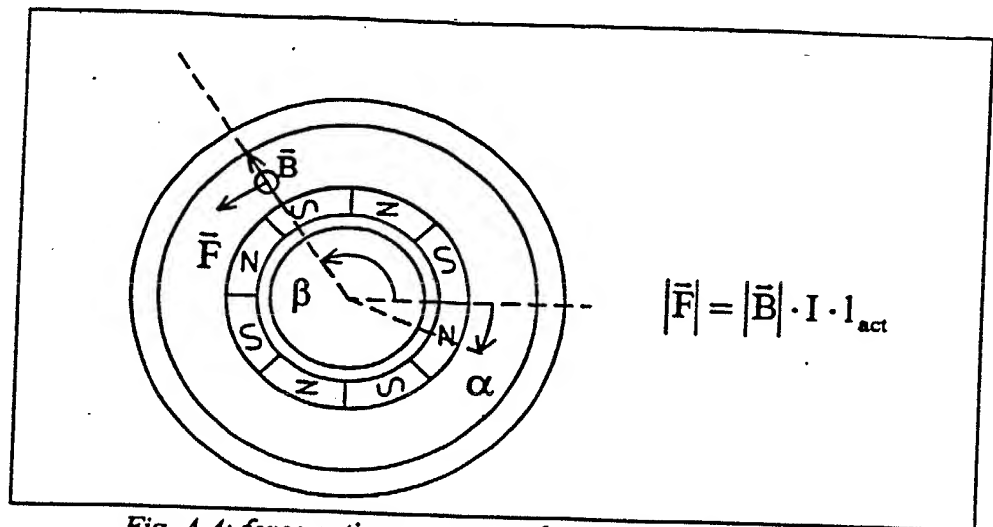
Fig. A.4: force acting on one conductor placed in the airgap

Fig. 3B

$$\vec{F}_{react} = -\vec{F}$$
$$|\vec{F}_{react}| = |\vec{F}|$$
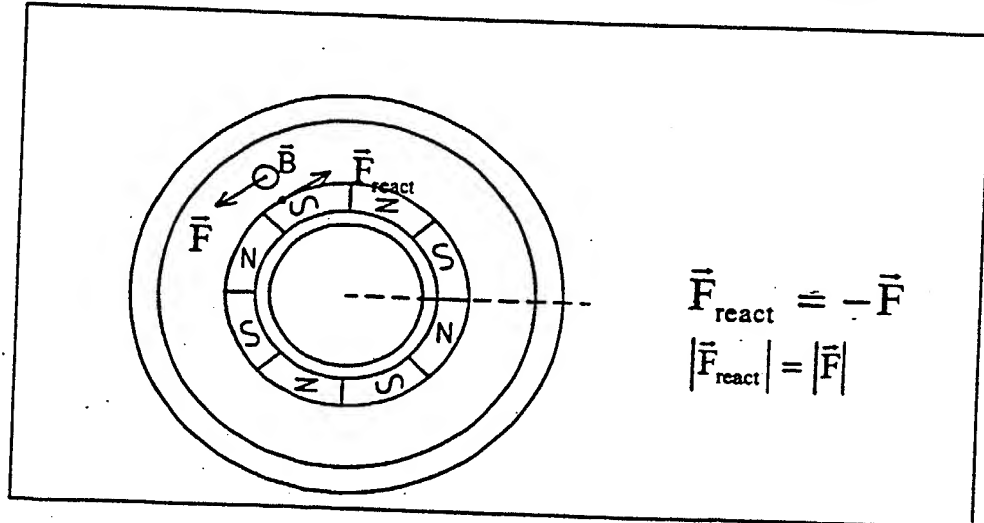
Fig. A.5: action and reaction rule, force acting on the magnet due to current flowing through the conductor placed in the airgap.

Fig. 4

$$\vec{F}_{react} \,\forall\, \left|\vec{F}_{react}\right| > 0$$

$$F_x = \left|\vec{F}_{react}\right| \cdot \sin(\beta)$$

$$F_y = \left|\vec{F}_{react}\right| \cdot \cos(\beta + \pi)$$

$$F_y = -\left|\vec{F}_{react}\right| \cdot \cos(\beta)$$

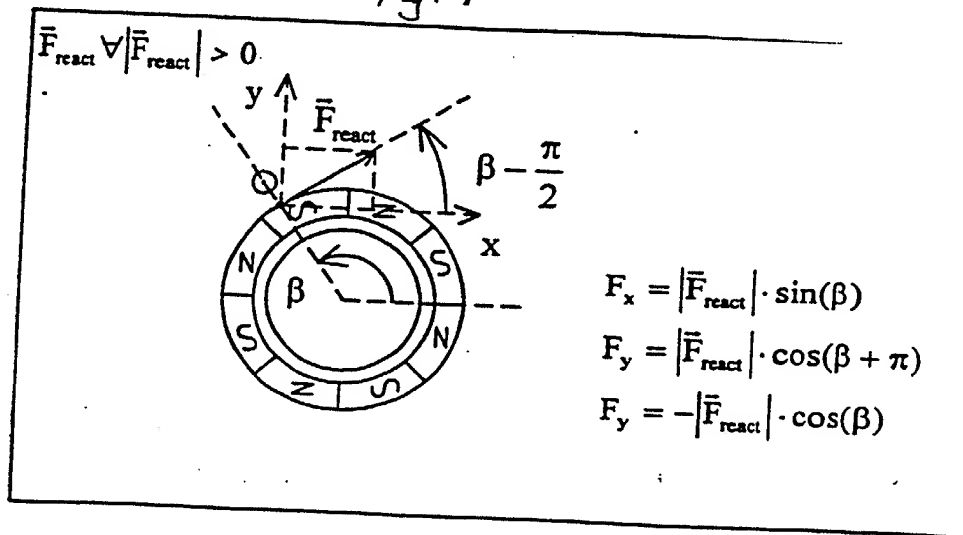Fig. A.6: projection of the force on the x and y axis.

Fig. 5
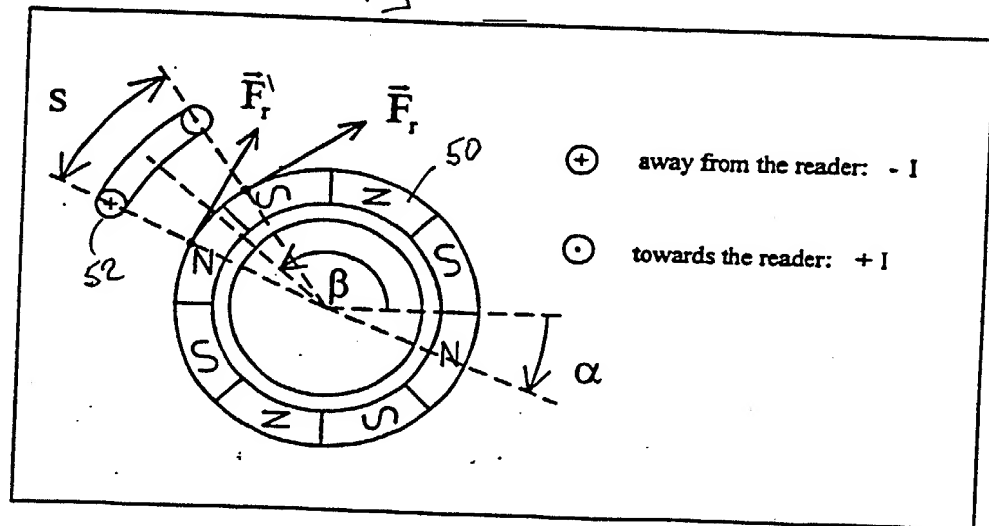
Fig. A.7: 2 forces acting on the magnet when one coil is placed in the airgap.

Fig 6A

Fig 6B

a: coil opening of 1 slot
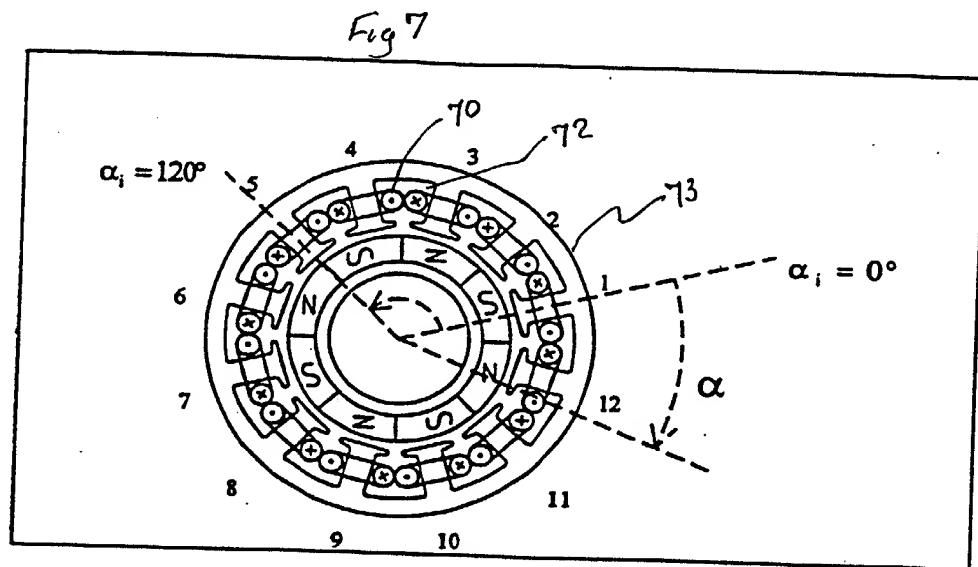
b: coil opening of 2 slots

Fig. A.8

Fig 7

Fig. A.10: 12 concentric coils placed in the 12 slots of the motor.
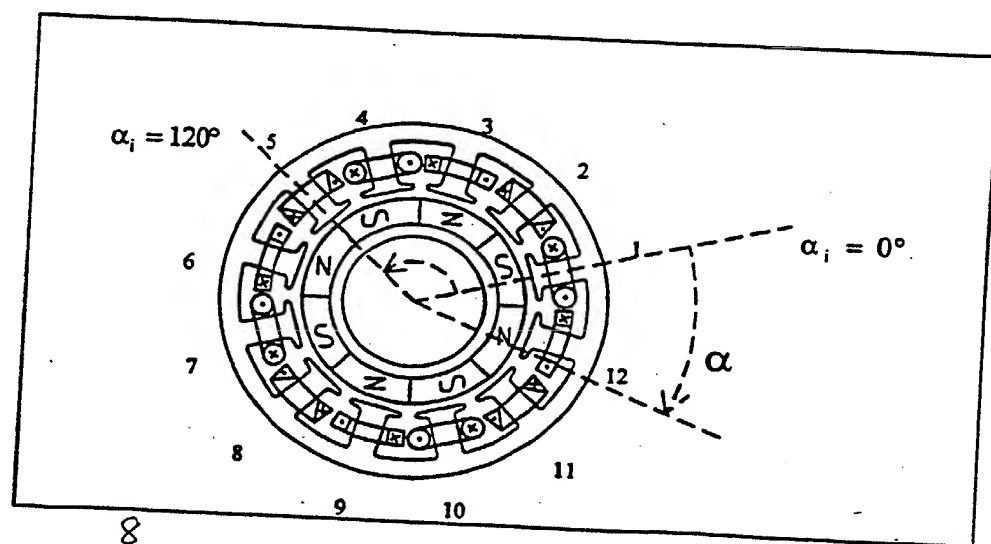
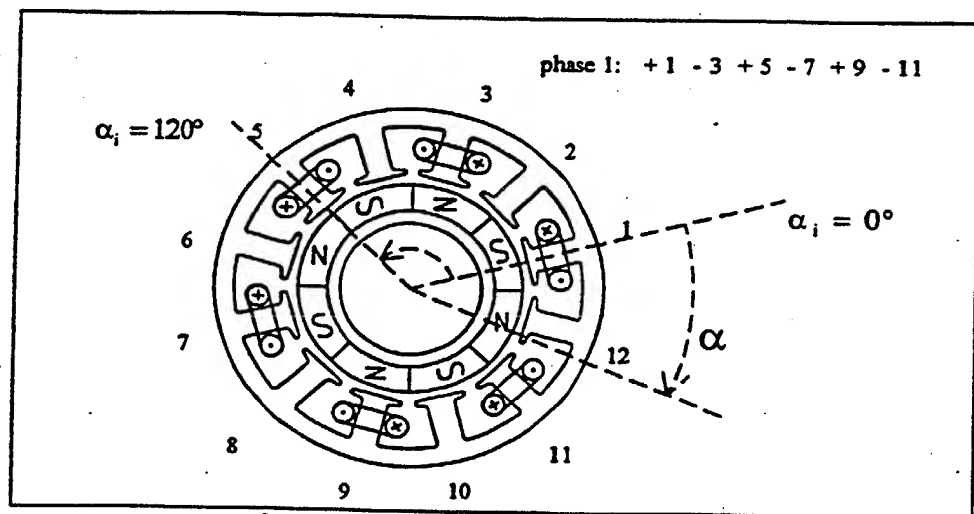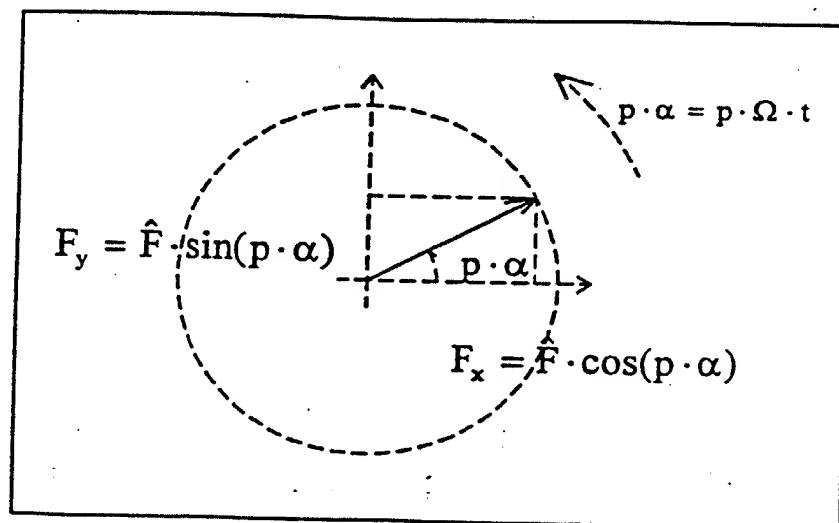Fig. A.12: *3 phase winding generating torque for a 8 poles 12 slots motor*

phase 1: + 1 - 3 + 5 - 7 + 9 - 11

$\alpha_i = 120°$

$\alpha_i = 0°$

α

Fig. A.14: one phase of 6 coils generating a radial force.

9

$$p \cdot \alpha = p \cdot \Omega \cdot t$$

$$F_y = \hat{F} \cdot \sin(p \cdot \alpha)$$

$$p \cdot \alpha$$

$$F_x = \hat{F} \cdot \cos(p \cdot \alpha)$$

10

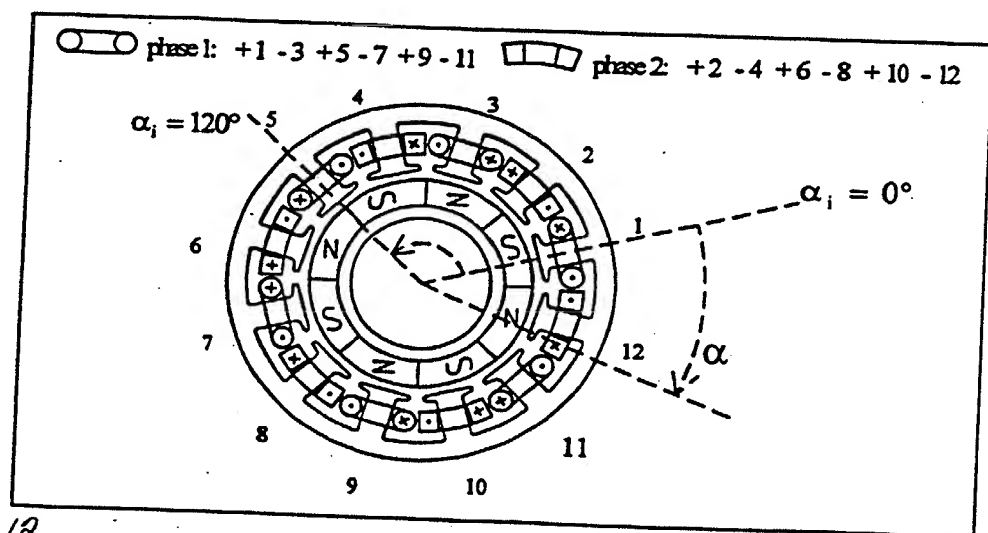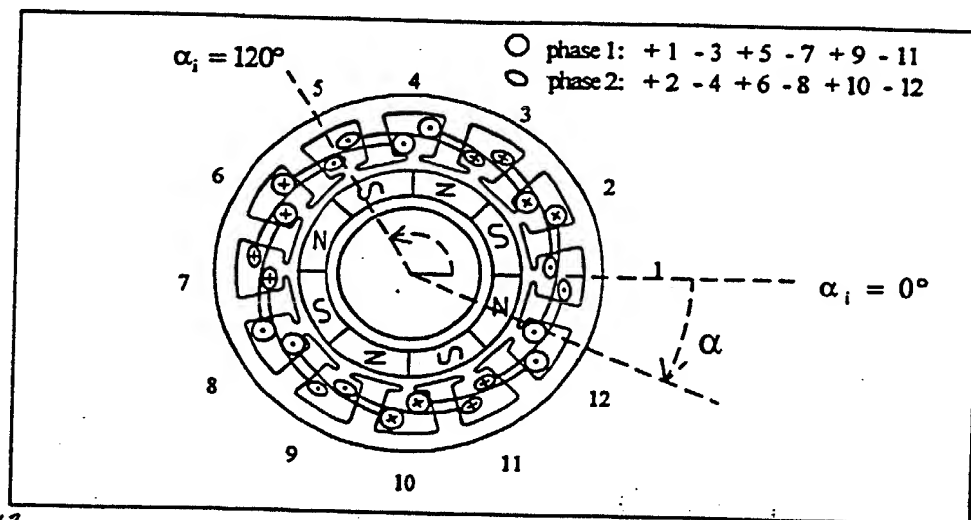*Fig. A.15: one rotating radial force.*
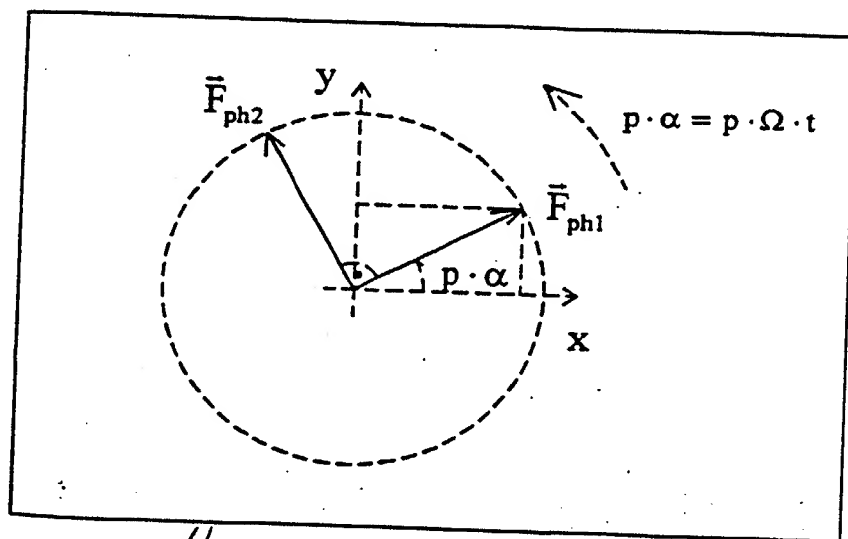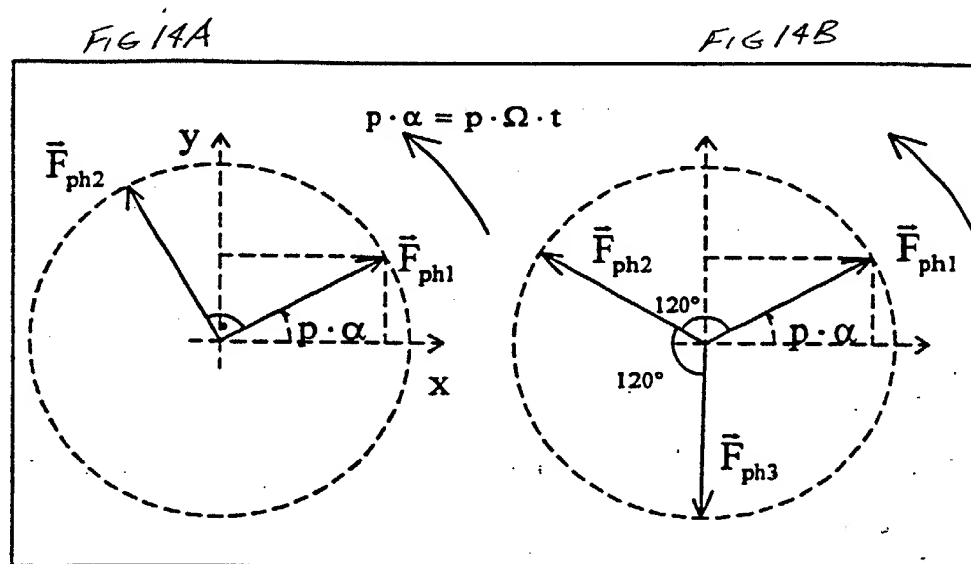
Fig. 4.16: 2 rotating radial forces in quadrature.

Fig. 4.18: 2 phase winding generating 2 radial forces in quadrature, coil opening of 1 slot.

$\alpha_i = 120°$

phase 1: $+1 \; -3 \; +5 \; -7 \; +9 \; -11$
phase 2: $+2 \; -4 \; +6 \; -8 \; +10 \; -12$

$\alpha_i = 0°$

α

13

Fig. A.19: 2 phase winding generating 2 radial forces in quadrature, coil opening of 2 slots.

FIG 14A   FIG 14B

$$p \cdot \alpha = p \cdot \Omega \cdot t$$

a: 2 rotating forces in quadrature.   *b: 3 rotating forces separated by 120°.*

Fig. 4.25

Fig. 15
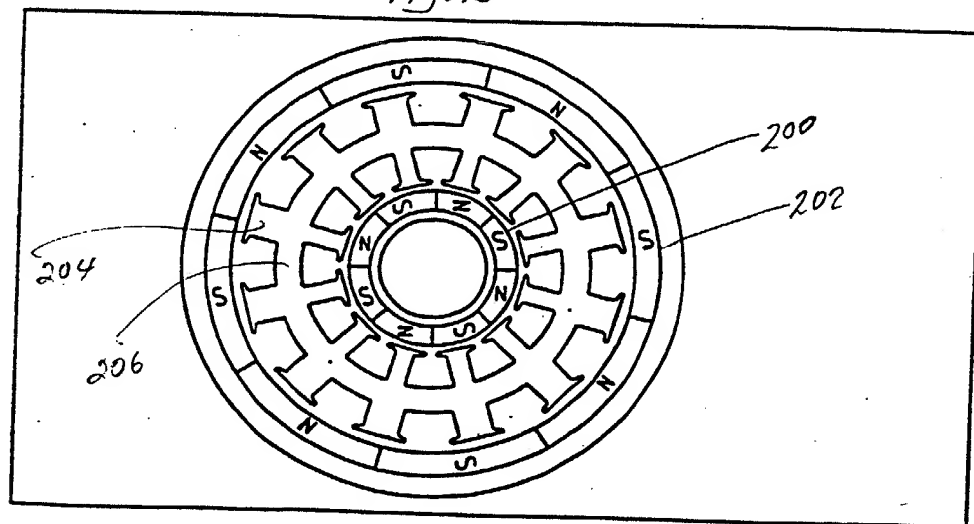
Fig. A.27: motor structure with 2 magnetic circuit.

Fig 16A

Fig. 16B

Glass fibre

16
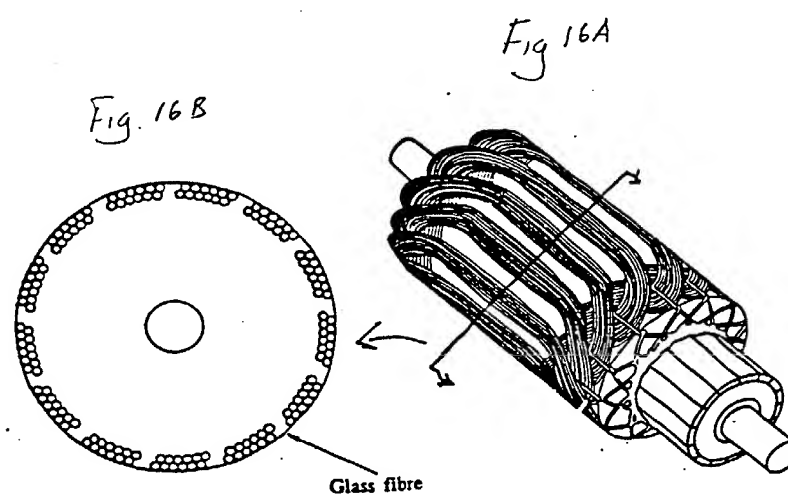
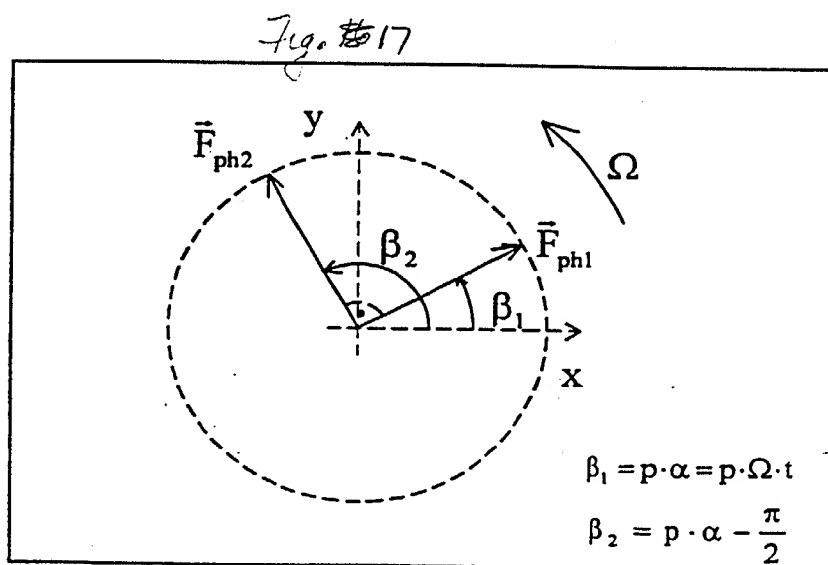Fig. 1.28: example of a slotless motor winding (cylinder placed in the airgap).

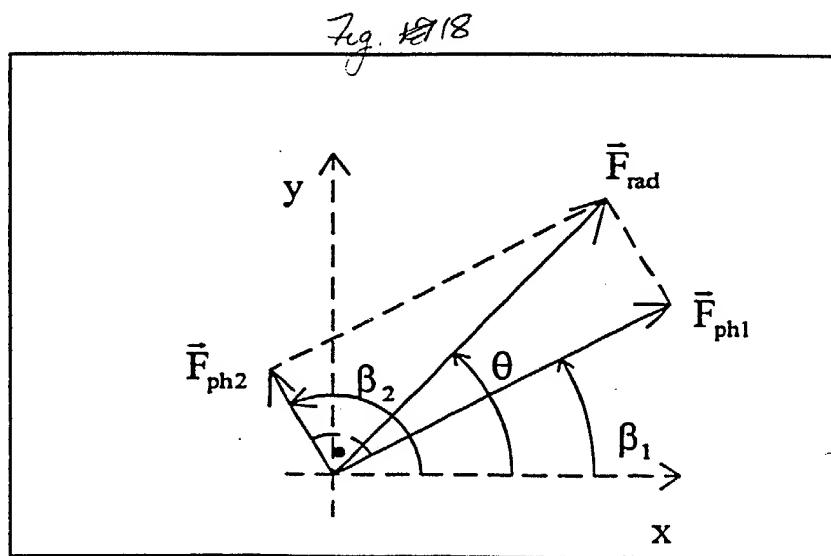*Fig. A.34*: *2 rotating radial forces in quadrature.*

Fig. A.35: projection of the radial force vector onto the vectors of the forces generated by phases 1 and 2.
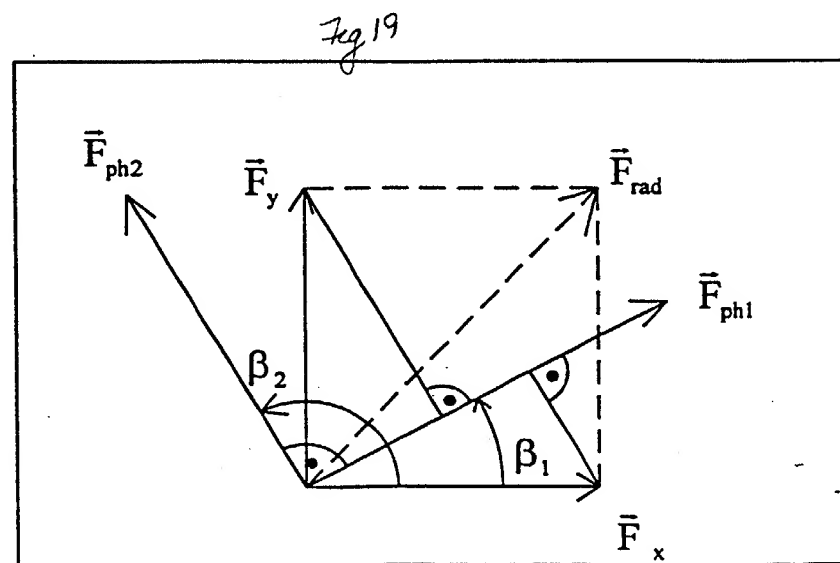
Fig 19

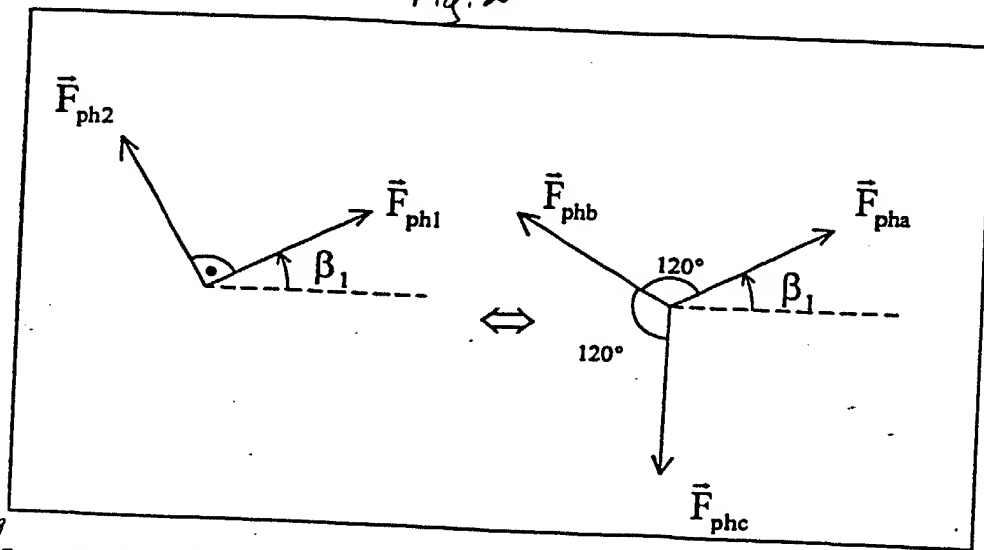Fig. A.36: *projections of the x and y radial force component vectors onto the vector of the force generated by phase 1.*

Fig. 20

$\vec{F}_{ph2}$

$\vec{F}_{ph1}$

β_1

$\Leftrightarrow$

$\vec{F}_{phb}$

120°

$\vec{F}_{pha}$

β_1

120°

$\vec{F}_{phc}$

Fig. ~~A.37~~: relationship between a sum of 2 forces in quadrature and a sum of 3 forces which directions are separated by 120°.

Fig. 21

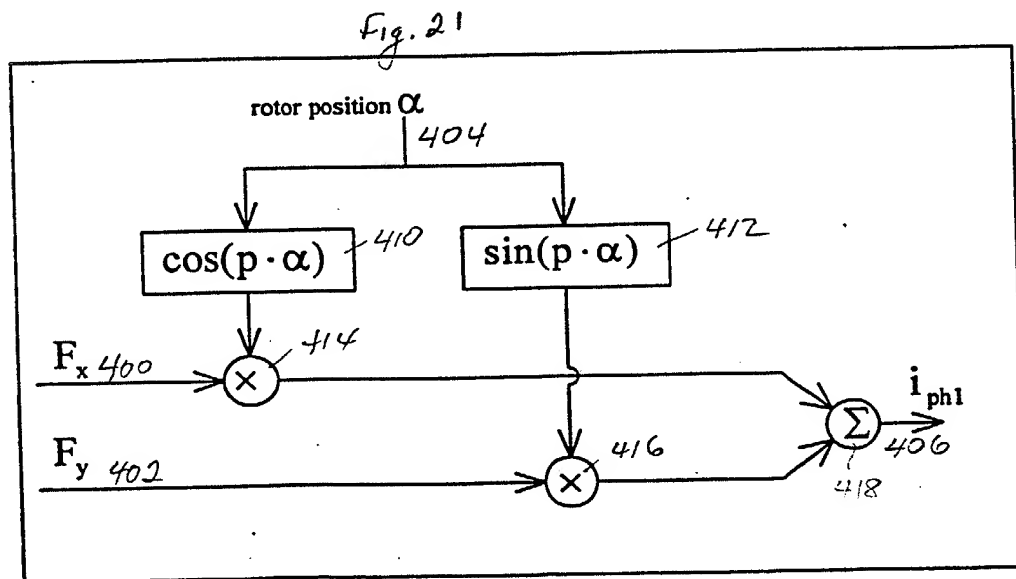Fig. A.38: bloc diagram of the phase 1 current calculation (expression (a.59)).

Fig 22

Reference Voltage *426*

$= F_x$

MEMORY
EPROM *420*

addresses
$= p \cdot \alpha$

data *424*

$sin(p\alpha)$

A *422*
D

Output Voltage
$= F_x \cdot sin(p\alpha)$
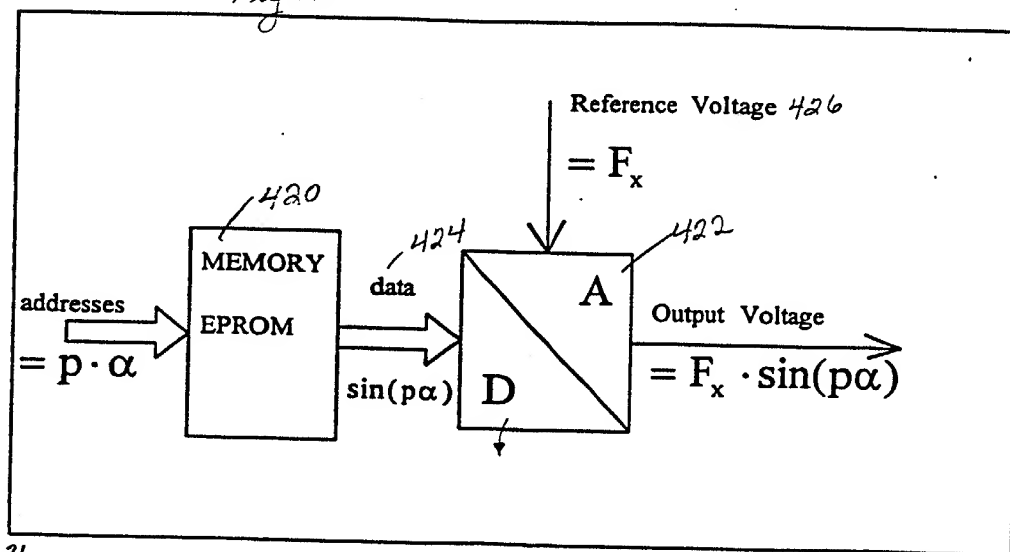
21
Fig. 22: electronic solution processing one trigonometric function and one multiplication.

Fig. 23

CK 442

frequency $= 256 \cdot \dfrac{\Omega}{2\pi} \cdot p$

440

counter

RESET

444

1 pulse per electrical period

addresses $= p \cdot \alpha$

Fig. A 40: electronic solution for generating the EPROM addresses
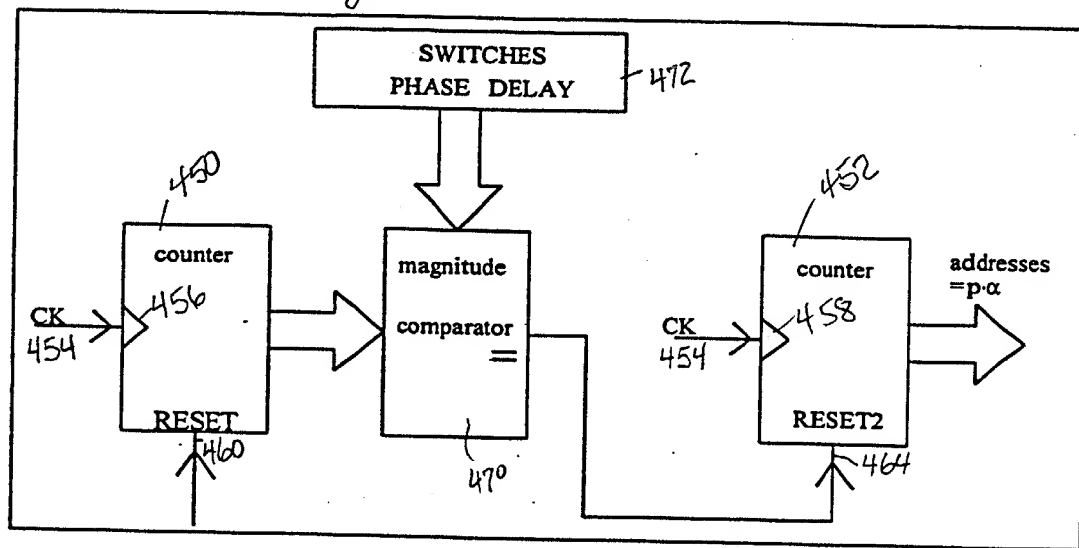as a function of the rotor position.
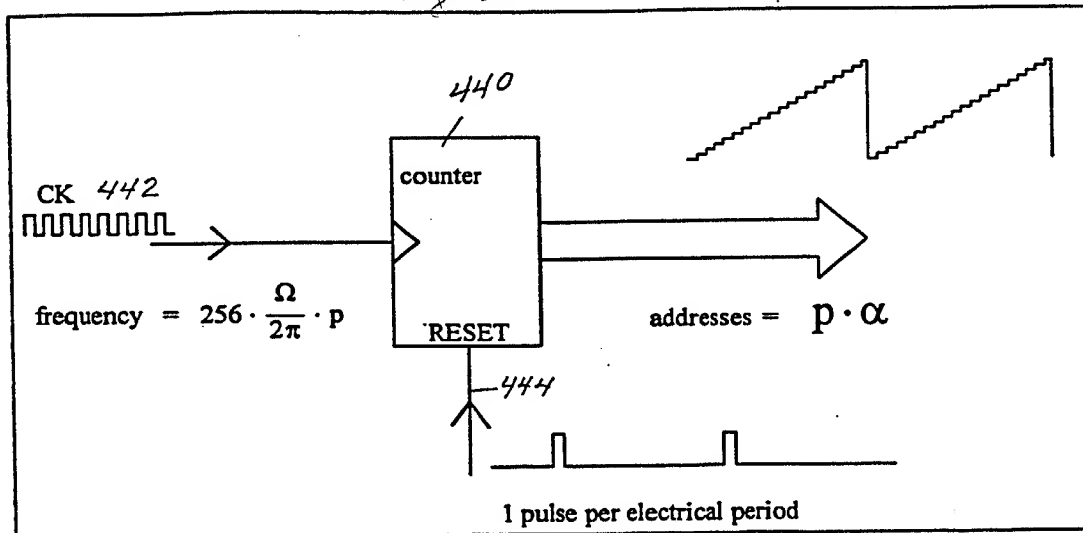
Fig 24

Fig. A.42: electronic solution generating the EPROM addresses as a function of the rotor position, with phase delay adjustment possibility
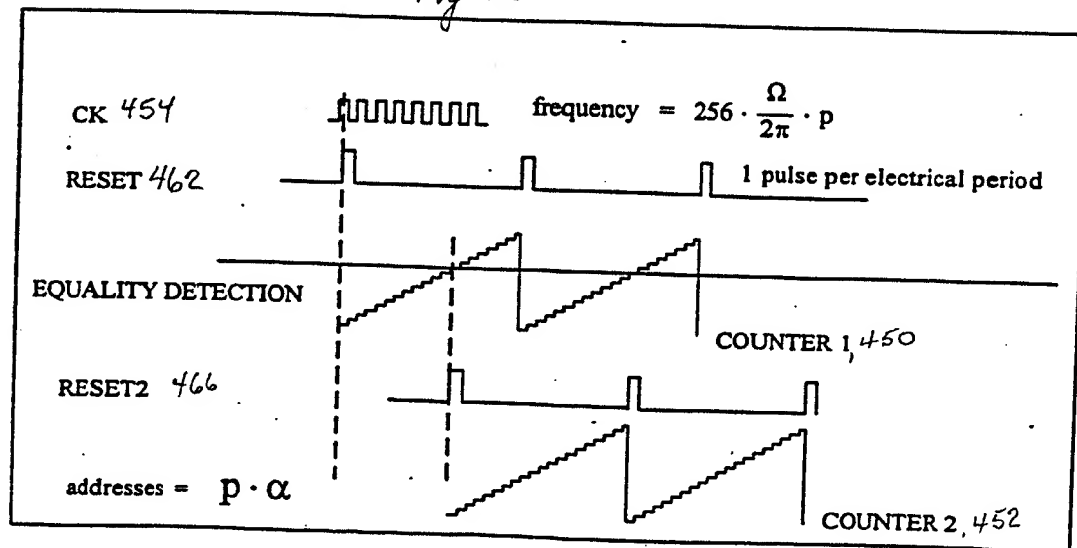
Fig 25

CK 454   ⊔⊔⊔⊔⊔⊔⊔   frequency = $256 \cdot \dfrac{\Omega}{2\pi} \cdot p$

RESET 462   1 pulse per electrical period

EQUALITY DETECTION

                                             COUNTER 1, 450

RESET2 466

addresses = $p \cdot \alpha$

                                             COUNTER 2, 452

Fig. A.43: Timing diagram corresponding to the electronic solution of Fig. A.42.

Fig 26

Hall element Amplifier   RESET   +Vcc

(a) Practical circuit of three-
phase bipolar driven motor, and
arrangement of Hall elements;
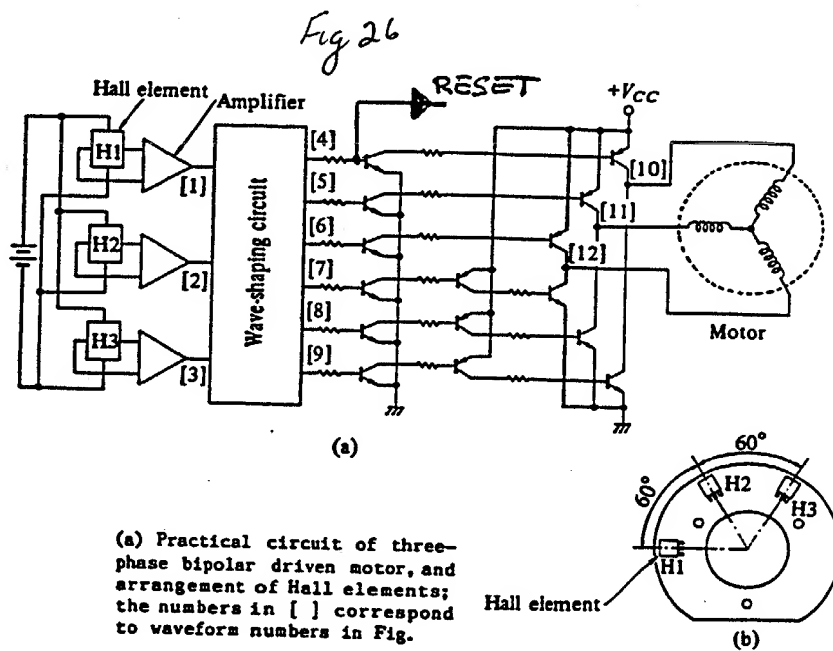the numbers in [ ] correspond
to waveform numbers in Fig.

Fig. A.44: Using a transistor command signal of the motor driver to generate one pulse per electrical period.

[1]

[2]

[3]

RESET

[4]

[5]

[6]

[7]

[8]

[9]

[10]

[11]

[12]

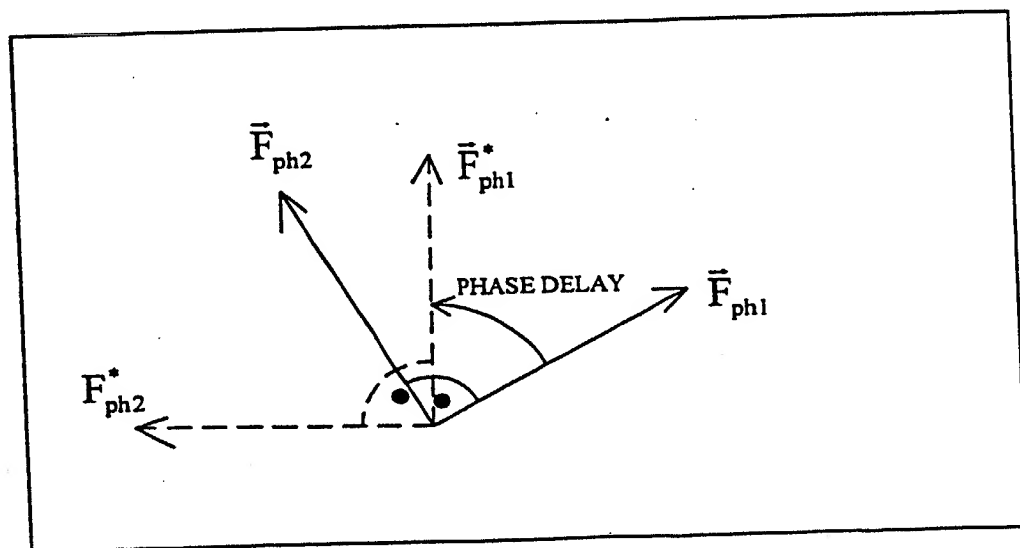| Mechanical angle | 0 | 90 | 180 | 270 | 360 |
| Electrical angle | 0 | 180 | 360 | 540 | 720 |
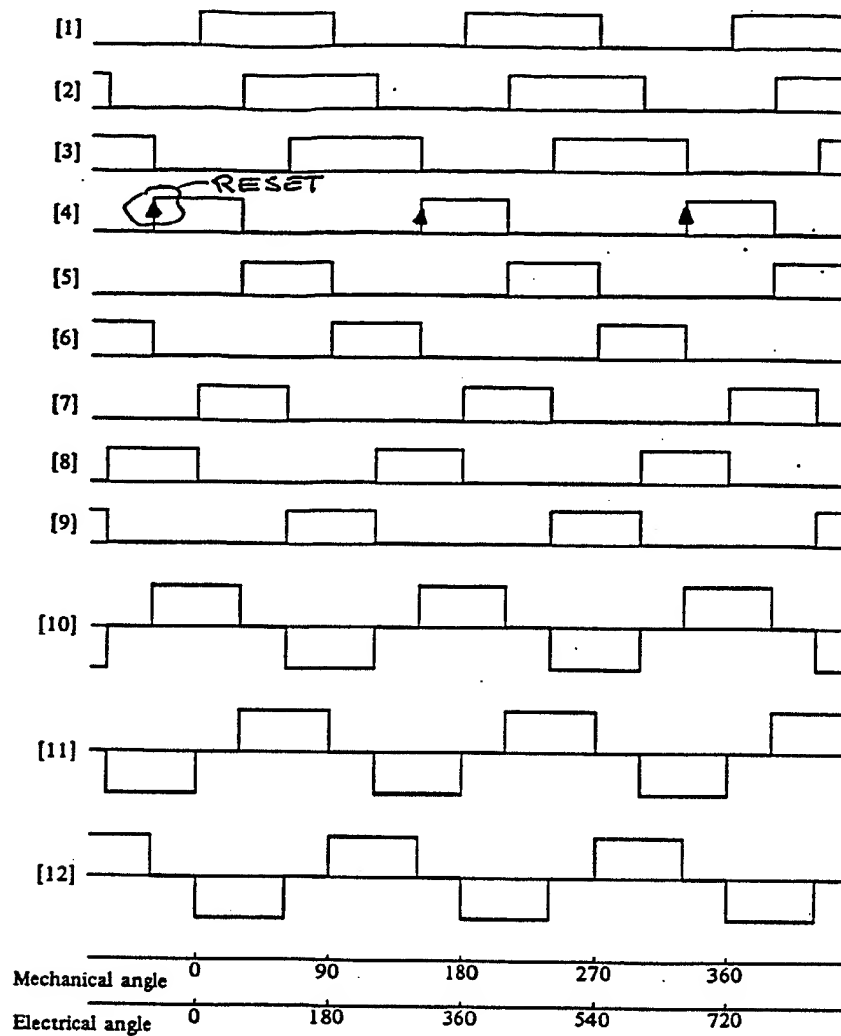
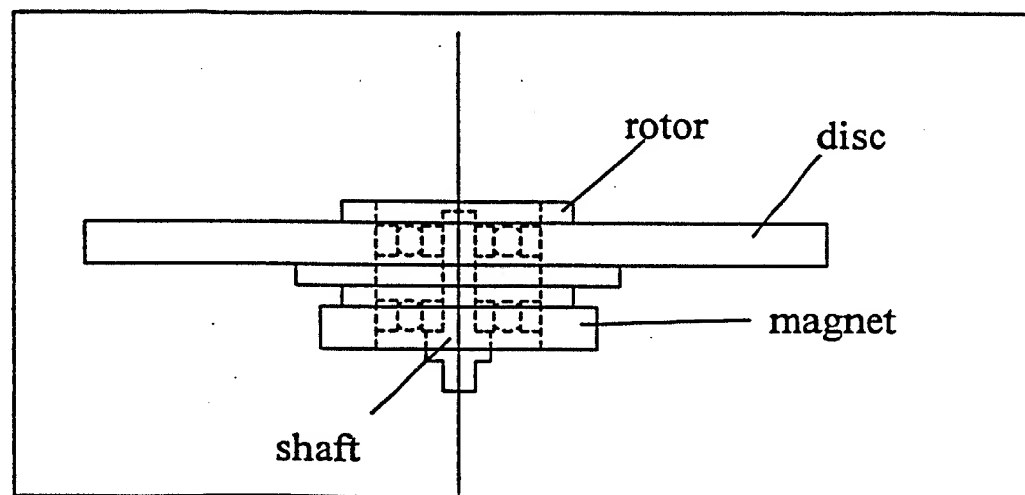Voltage waveforms at each part (see Fig. A.44(a)).

27

Fig. A.45: *Using a transistor command signal of the motor driver to generate one pulse per electrical period, timing diagram.*
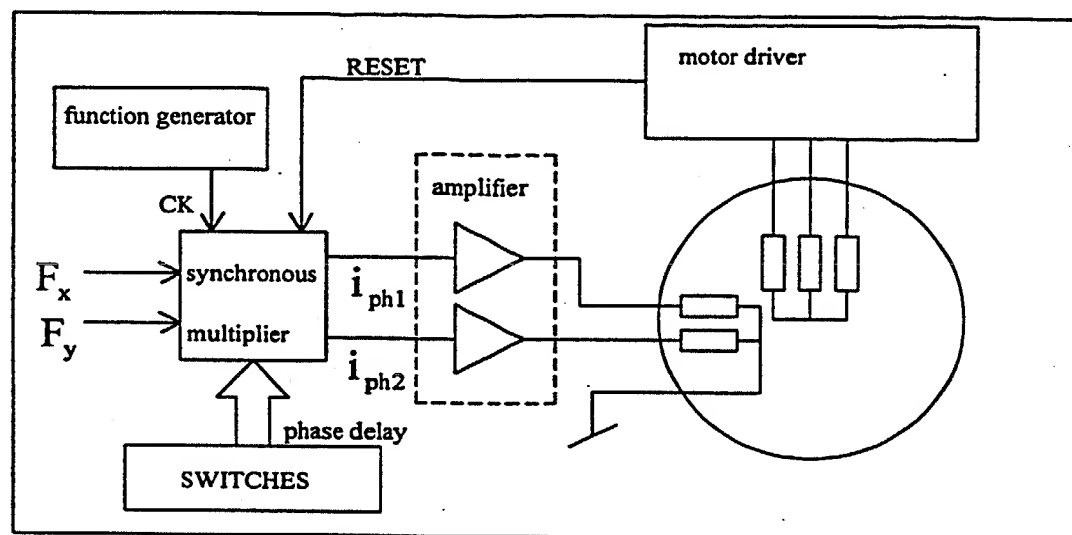
28

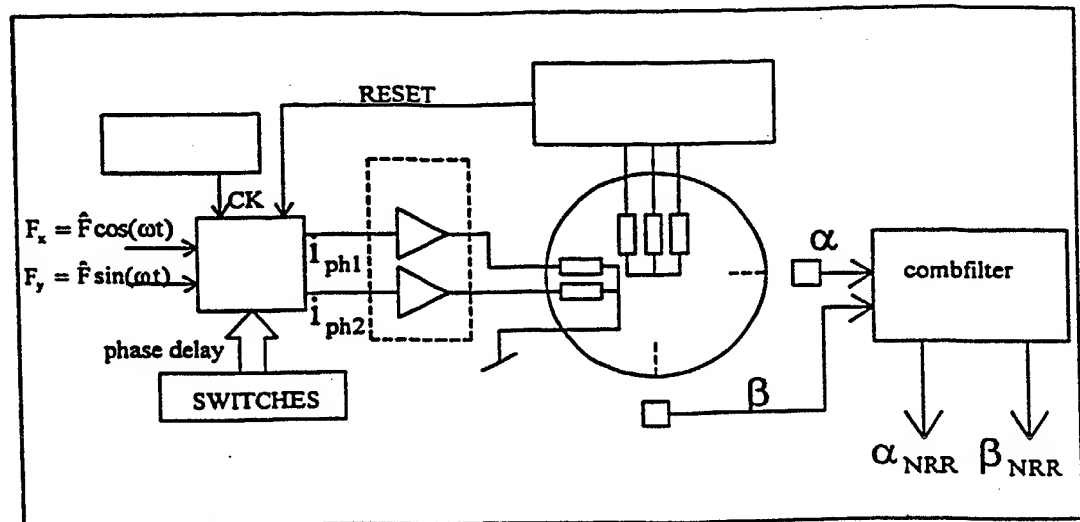*Fig. A.46: final bloc diagram of the electronic supply of the 2 phase winding generating radial force .*

29

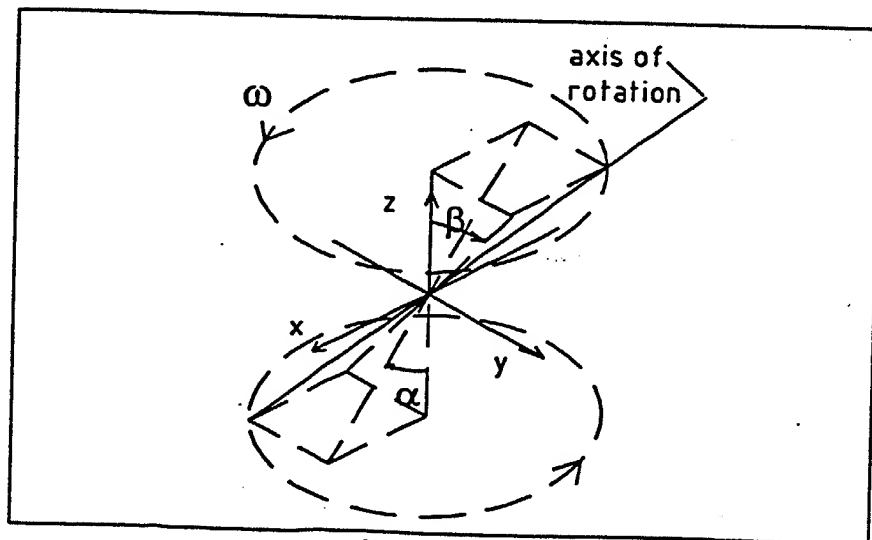Fig. ~~A.47~~: *phase delay effect on the radial force direction.*

rotor   disc

magnet

shaft

30

Fig. A.48: harddrive spindle motor.

31

Fig. A.49: measurement of the response to a rotating radial force excitation.

32

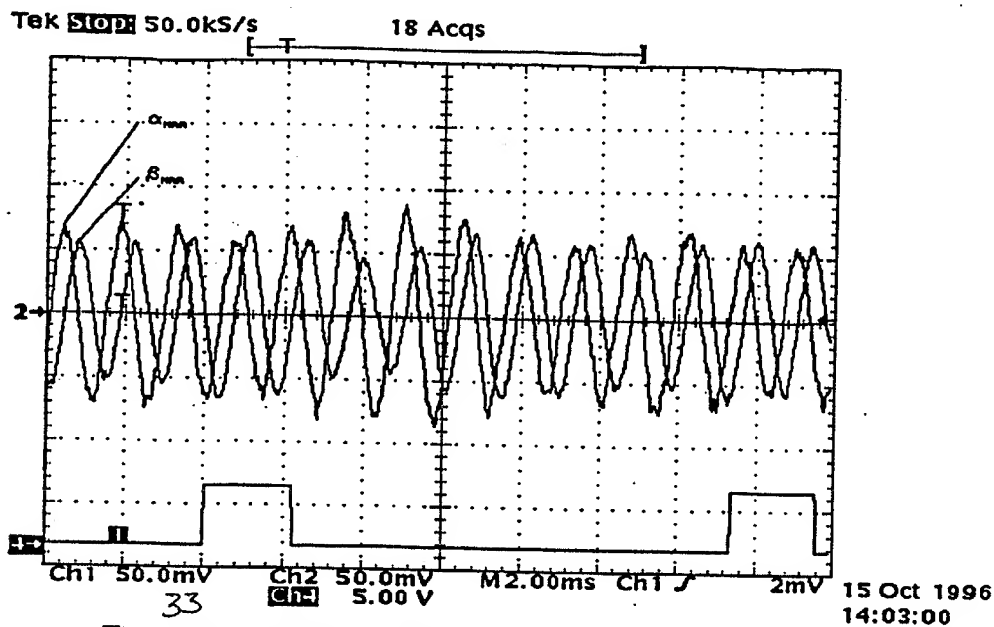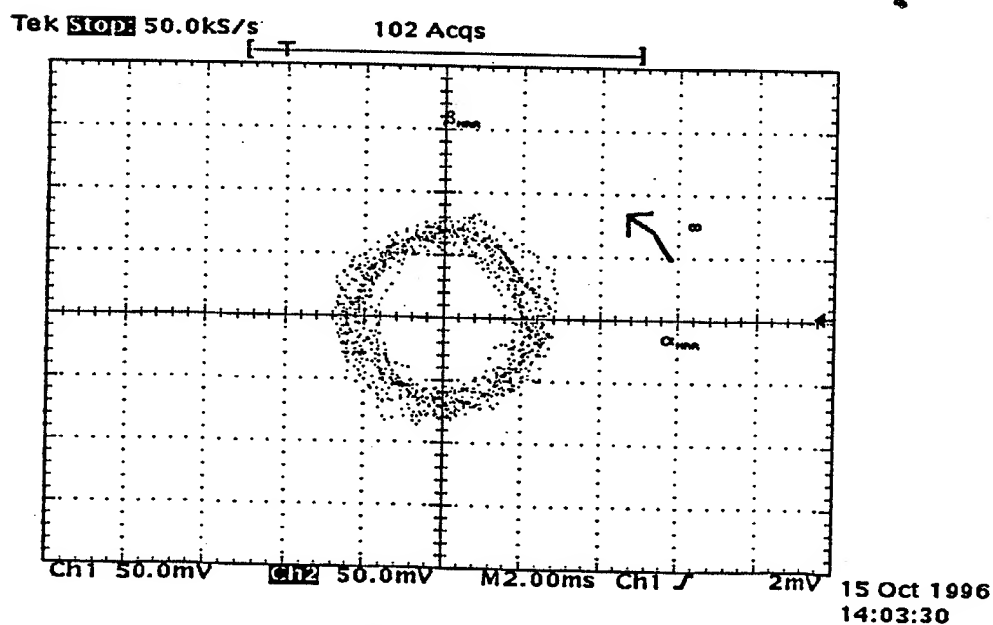*Fig. A.50: definition of the rotational axis angular position*

Fig. A.51: *excitation of the forward gyroscopic mode, measure of the NOR components of* α *and* β, *measure of a signal giving one pulse per revolution.*

Fig. A.52: *excitation of the forward gyroscopic mode,*
Lissajou figure of the NRR components of α *and* β.

Ch1 50.0mV   Ch2 50.0mV   M2.00ms Ch1 ⌐   2mV   15 Oct 1996
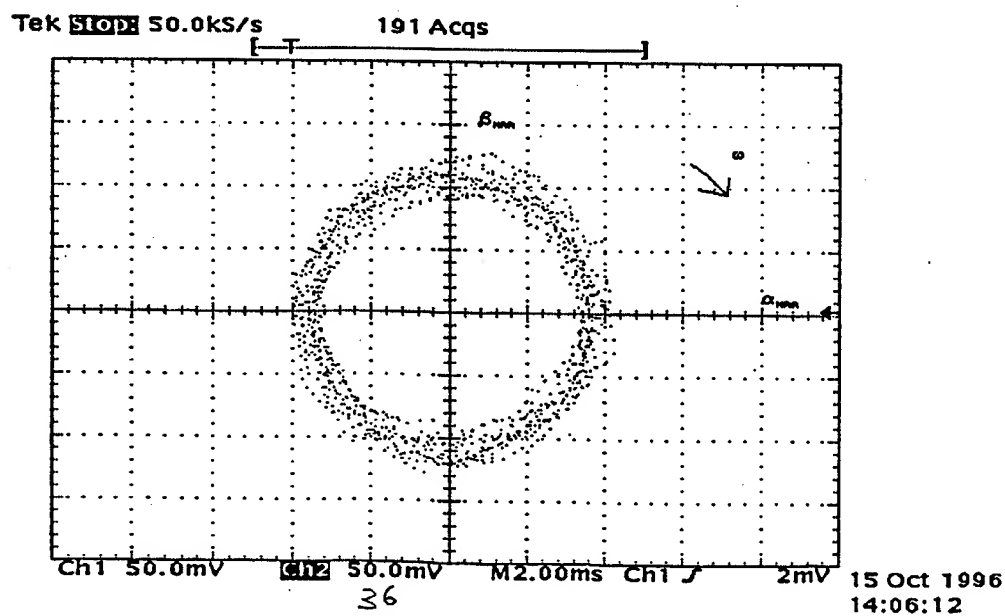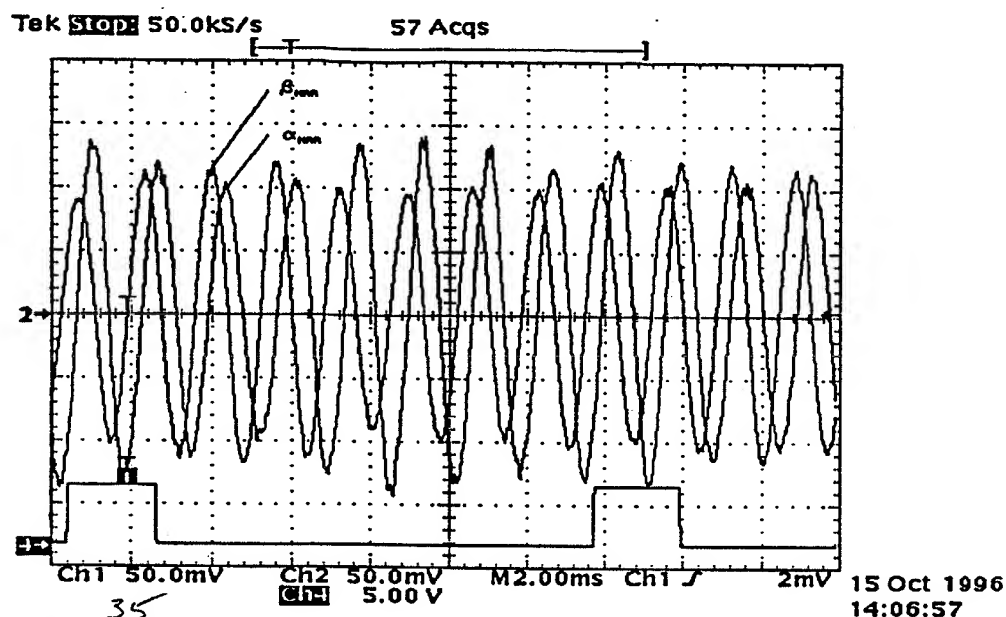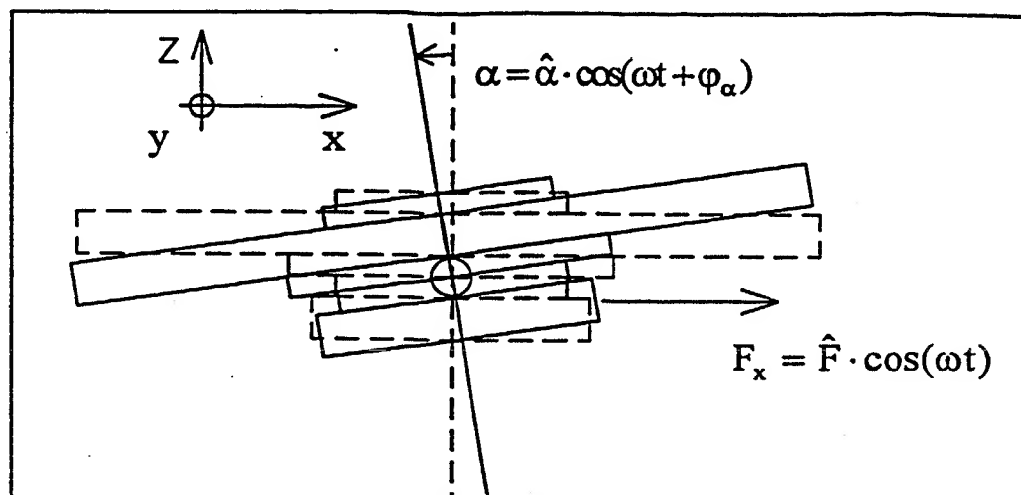   **Ch4** 5.00 V   14:06:57

35

Fig. A.53: excitation of the backward gyroscopic mode, measure of the NRR components of α
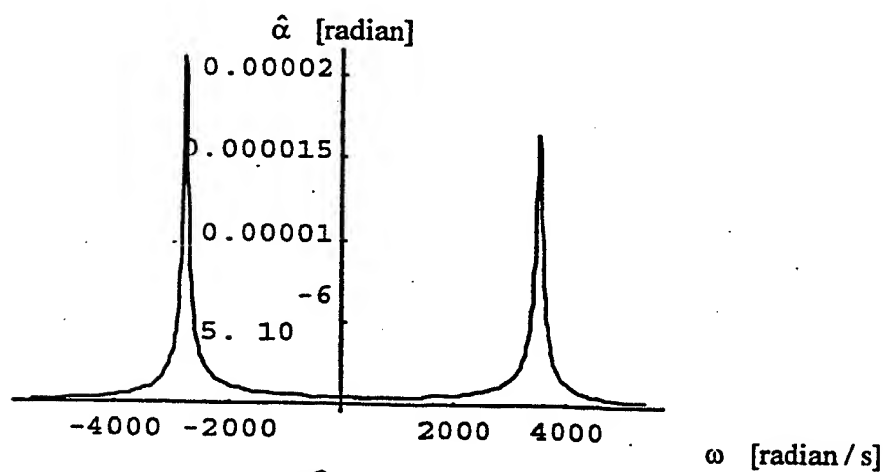*and* β, *measure of a signal giving one pulse per revolution.*

Ch1 50.0mV   **Ch2** 50.0mV   M2.00ms Ch1 ⌐   2mV   15 Oct 1996
                                                                    14:06:12

36

Fig. A.54: excitation of the backward gyroscopic mode,
Lissajou figure of the NRR components of α *and* β.

$$\alpha = \hat{\alpha} \cdot \cos(\omega t + \varphi_\alpha)$$

$$F_x = \hat{F} \cdot \cos(\omega t)$$

37

Fig. A.55: rotor motion in plan xz.

$\hat{\alpha}$ [radian]

0.00002

0.000015

0.00001

5. 10^{-6}

-4000 -2000   2000 4000

ω [radian / s]

38

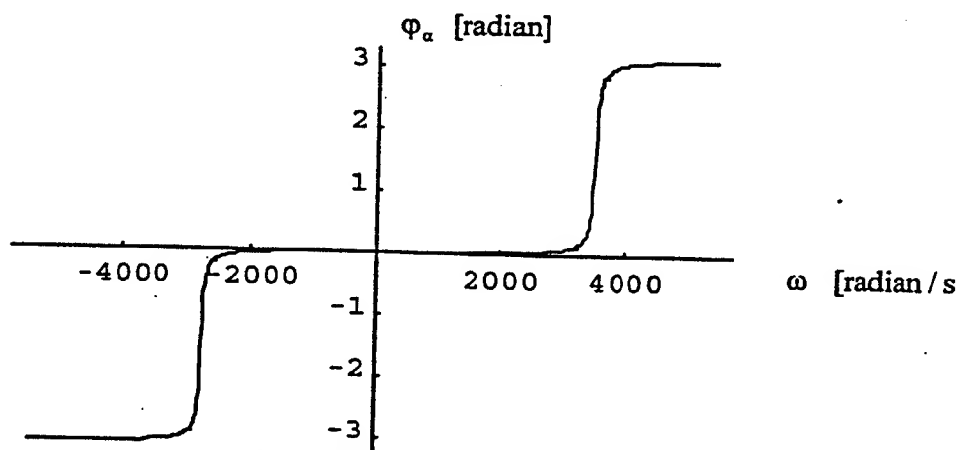Fig. A.56: Bode plot of the α wave magnitude.

Fig. A.57: Bode plot of the α wave phase delay.

39

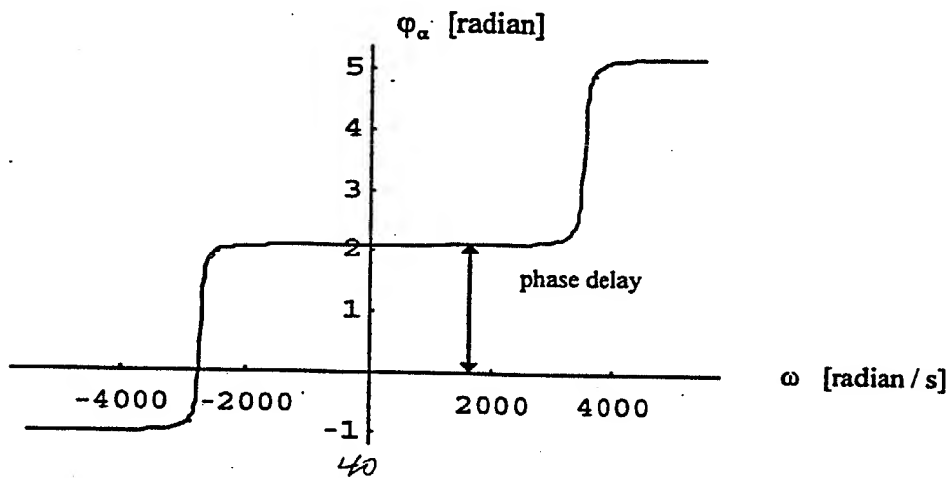Fig. 4.58: Bode plot of the α wave phase delay including
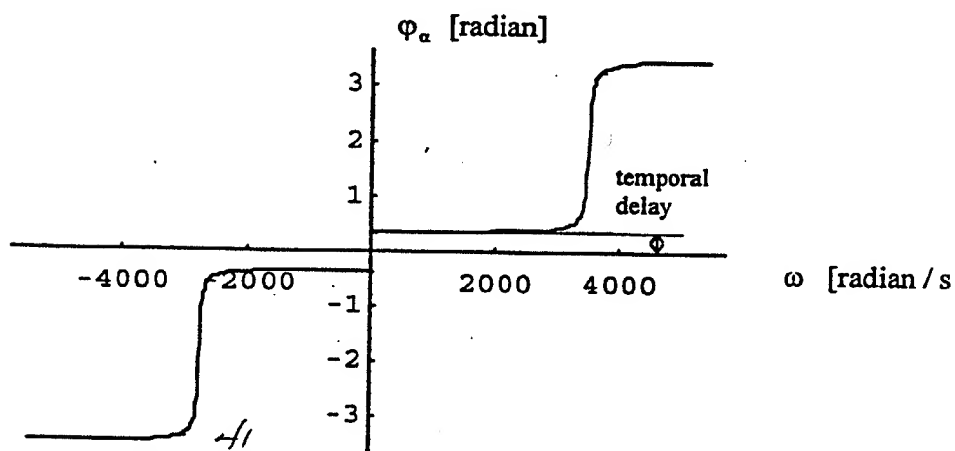the effect of the synchronous multiplier phase delay.
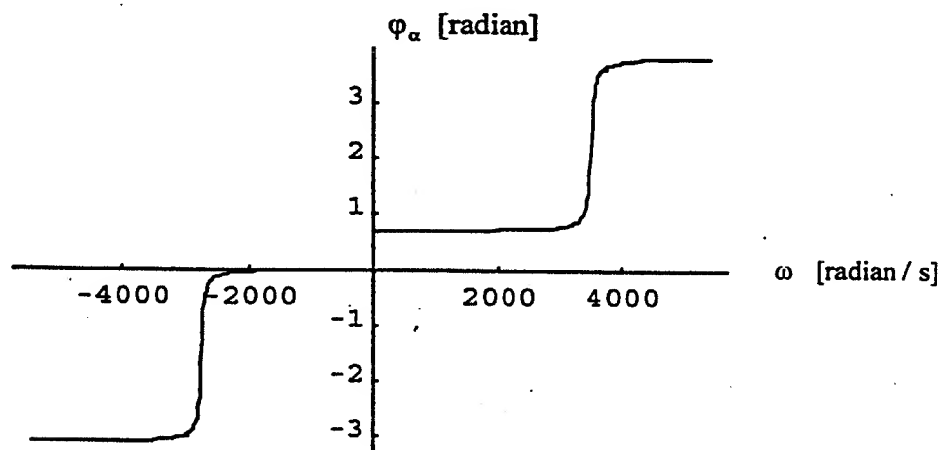
Fig. A.59: Bode plot of the α wave phase delay, including the temporal delay
introduced by the current amplifiers and by the measure system.

Fig. A 60: correction of the temporal delay of the backward gyroscopic mode with the synchronous multiplier phase delay.